RESEARCH ARTICLE

Revisiting chemoaffinity theory: Chemotactic implementation of topographic axonal projection

Honda Naoki*

Graduate School of Biostudies, Kyoto University, Sakyo, Kyoto, Japan

* n-honda@sys.i.kyoto-u.ac.jp

Abstract

Neural circuits are wired by chemotactic migration of growth cones guided by extracellular guidance cue gradients. How growth cone chemotaxis builds the macroscopic structure of the neural circuit is a fundamental question in neuroscience. I addressed this issue in the case of the ordered axonal projections called topographic maps in the retinotectal system. In the retina and tectum, the erythropoietin-producing hepatocellular (Eph) receptors and their ligands, the ephrins, are expressed in gradients. According to Sperry's chemoaffinity theory, gradients in both the source and target areas enable projecting axons to recognize their proper terminals, but how axons chemotactically decode their destinations is largely unknown. To identify the chemotactic mechanism of topographic mapping, I developed a mathematical model of intracellular signaling in the growth cone that focuses on the growth cone's unique chemotactic property of being attracted or repelled by the same guidance cues in different biological situations. The model presented mechanism by which the retinal growth cone reaches the correct terminal zone in the tectum through alternating chemotactic response between attraction and repulsion around a preferred concentration. The model also provided a unified understanding of the contrasting relationships between receptor expression levels and preferred ligand concentrations in EphA/ephrinA- and EphB/ephrinB-encoded topographic mappings. Thus, this study redefines the chemoaffinity theory in chemotactic terms.

Author summary

This study revisited the chemoaffinity theory for topographic mapping in terms of chemotaxis. According to this theory, the axonal growth cone projects to specific targets based on positional information encoded by chemical gradients in both source and target areas. However, the mechanism by which the chemotactic growth cone recognizes its proper terminal site remains elusive. To unravel this mystery, I mathematically modeled a growth cone exhibiting concentration-dependent attraction and repulsion to chemotactic cues. The model identified a novel growth cone guidance mechanism in topographic mapping, highlighting the importance of the growth cone's unique ability to alternate between

attraction and repulsion. Furthermore, an extension of the model provided possible molecular mechanisms for contrasting two types of topographic mappings observed in the retinotectal system.

Introduction

During development, neurons extend axon and dendrites [1–3] and axonal growth cones chemotactically migrate in response to extracellular guidance cue gradients and connect to their target sites. Because this axon guidance is a fundamental process in wiring neural circuits, many guidance cues and receptors have been identified and their functional roles (e.g., attraction or repulsion) have been extensively investigated [4–6]. The growth cone's chemotactic properties are thus being unveiled at the molecular level, but the chemotactic mechanisms of neural circuit construction remain mysterious at the macroscopic level. I addressed this issue by investigating topographic maps, the ordered axonal projections ubiquitous in the sensory nervous system. The best-studied example is in visual system, where retinal ganglion cells (RGCs) project their axons to the optic tectum and/or superior colliculus (SC) while keeping an initial positional relation [7].

The most important concept of topographic map formation is the "chemoaffinity theory" proposed by Roger Sperry in 1940s [8]. Sperry proposed that chemical labels form gradients in source and target areas, allowing a projecting axon to recognize its target site. The theory's molecular basis was identified with the discovery of gradients of erythropoietin-producing hepatocellular (Eph) receptors and their ligands, ephrins, in the retina (source area) and tectum (target area) [9,10]. Ephs and ephrins are classified into two families, A and B, that encode orthogonal topographic maps in the retina and tectum (**Fig 1**).

The EphA receptor gradient along the retina's nasal-temporal axis topographically corresponds to the ephrinA gradient along the tectum's rostral-caudal axis (**Fig 1A**). On the orthogonal coordinates, the EphB receptor gradient along the retina's dorsal-ventral axis corresponds to the ephrinB gradient along the tectum's medial-lateral axis (**Fig 1C**). These facts suggest that RGC growth cones chemotactically migrate to their terminal zones guided by ligand concentrations reflective of receptor expression levels. Because ephrinA and ephrinB act as both attractants and repellents in a concentration-dependent manner [11–13], it is possible that growth cones switch between attraction and repulsion around the terminal zone, but the chemotactic mechanism for decoding destination from dual gradients (i.e., receptor and ligand) is unknown.

The EphA/ephrinA- and EphB/ephrinB-encoded topographic maps differ in that the RGCs with higher EphA receptor expression prefer lower tectal ephrinA concentrations (**Fig 1B**), whereas the RGCs with higher EphB receptor expression prefer higher tectal ephrinB concentrations (**Fig 1D**). In other words, the retinotectal system's two kinds of topographic mapping have opposite receptor expression-dependent ligand concentration preferences. How the growth cone's chemotactic system implements these opposite preferences is also unknown.

Topographic mapping has been extensively investigated with computational models for four decades [14], but all previous models featured growth cones reaching their terminal zones by heuristically-designed chemoaffinity [15–25]. While these models provided insights into the outcomes of surgical experiments in the retinotectal system [15–17] and the abnormal maps resulting from misexpression of Ephs or ephrins [15,18–25], none addressed how the intracellular mechanism of growth cone chemotaxis achieves chemoaffinity.
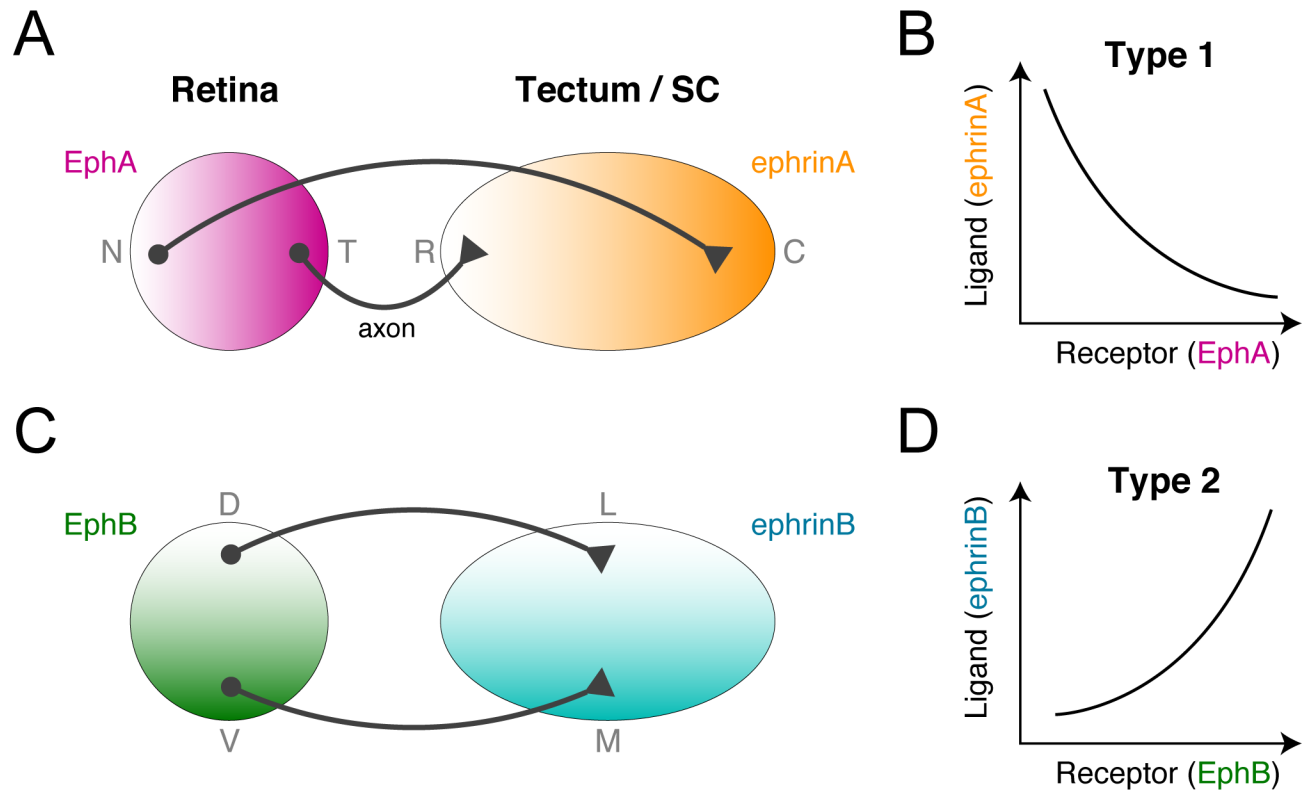
Fig 1. Two types of topographic maps in the retinotectal system. (A, B) Topographic mapping from the retina to the tectum is encoded by orthogonal gradients of EphA and EphB receptors in the retina and of their ligands, ephrinA and ephrinB, in the tectum or SC. **(C, D)** The EphA/ephrinA- and EphB/ephrinB-encoded topographic mappings exhibit opposite receptor expression level-dependent ligand concentration preferences. These were categorized as types 1 and 2 in this study.

I sought to determine the underlying mechanism of topographic mapping implemented by growth cone chemotaxis. To this end, I focused on the growth cone's unique chemotactic property of being attracted and repelled by the same guidance cues in different biological environments [26,27]. By mathematically modeling growth cone migration regulated by intracellular signaling, I attempted to demonstrate how the growth cone reaches its terminal zone in the tectum by switching attraction and repulsion around a preferred ligand concentration. Through this model, I redefined Sperry's chemoaffinity theory in terms of chemotaxis.

Results

I first studied the projecting growth cone's preference for a specific ligand concentration associated with the correct terminal zone in the target area. The basic idea is that a growth cone switches between attraction and repulsion around a specific preferred concentration; if the growth cone exhibits attraction and repulsion to lower and higher concentrations, respectively, then it ultimately reaches a location with the preferred concentration. To examine this idea, I mathematically modeled intracellular signaling in chemotactic growth cones.

Model of bidirectional chemotactic response

The model growth cone was equipped with an intracellular activator (A) and inhibitor (I) of their effector (E), where A and I were upregulated by guidance cues and E regulates the growth cone motility (**Fig 2A and 2B**). This activator-inhibitor framework has been commonly

observed in both neural and non-neural chemotactic cells [28–31]. For simplicity, a one-dimensional coordinate (x) across the growth cone was modeled as $\{x| -L/2 \leq x \leq L/2\}$, where L indicates its length. The reaction-diffusion dynamics of A and I were described by

$$\frac{\partial A}{\partial t} = D_A \frac{\partial^2 A}{\partial x^2} - k_A A + c_A + \alpha_A G(x)$$

$$\frac{\partial I}{\partial t} = D_I \frac{\partial^2 I}{\partial x^2} - k_I I + c_I + \alpha_I G(x)$$

(1)
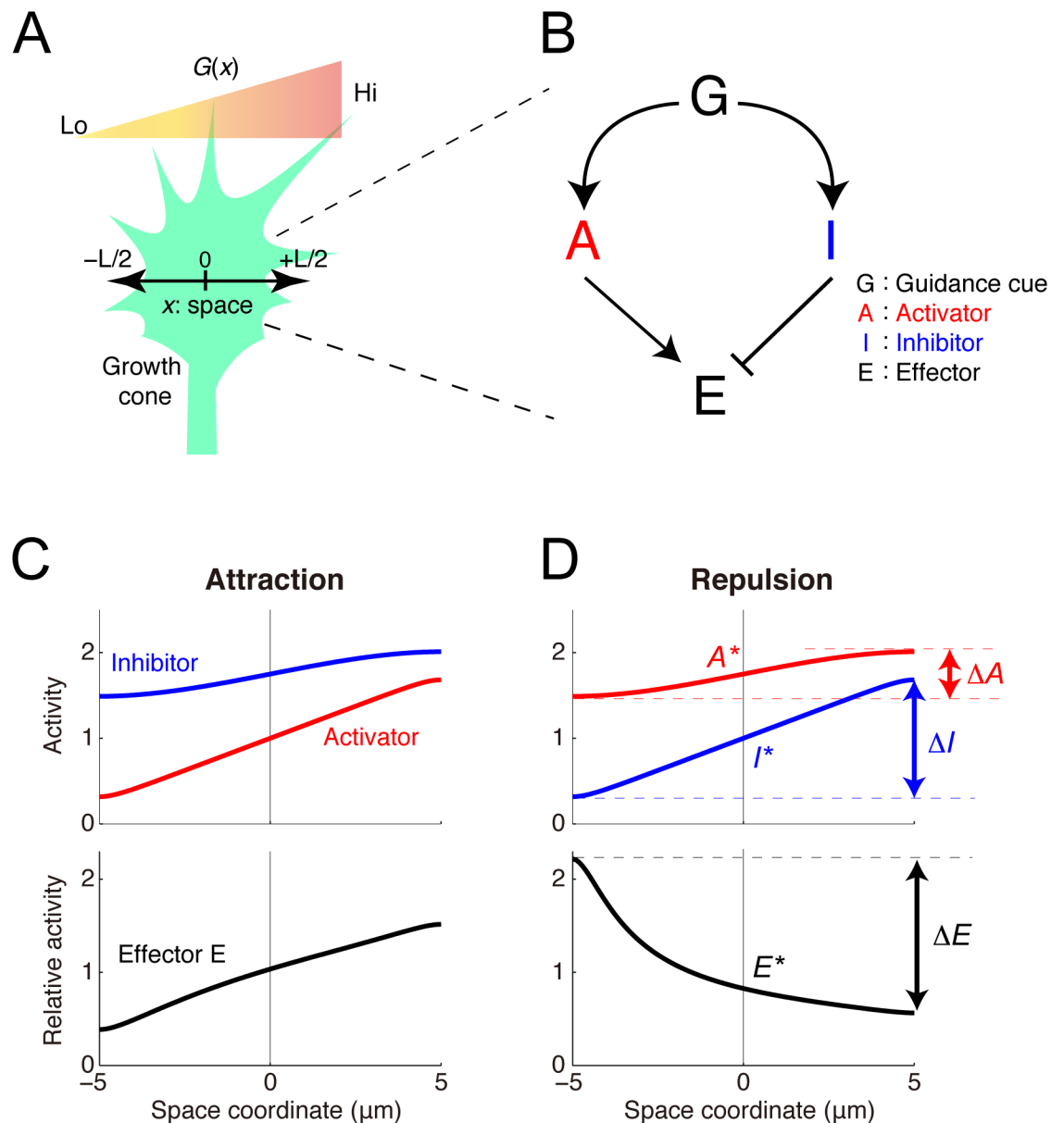
Fig 2. The model of the intracellular growth cone chemotactic process. (A) A schematic of the one-dimensional model growth cone encountering an extracellular gradient of guidance cues. **(B)** The model growth cone's components: a guidance cue (G) regulates an activator (A) and an inhibitor (I) of the effector (E). **(C, D)** Following exposure to a linear extracellular gradient of G ($G(x) = G^* + gx$), gradients of A and I are formed across the growth cone, thereby forming a gradient of E. If the gradient of E orients to the extracellular gradient ($\Delta E > 0$), then the growth cone shows attraction (C), but otherwise ($\Delta E < 0$), it shows repulsion (D). The model parameters are listed in **Table 1**.

https://doi.org/10.1371/journal.pcbi.1005702.g002

with reflecting boundaries at both ends ($x = \pm L/2$), where A and I represent the activities of A and I, respectively, D_Z, k_Z, c_Z, and α_Z ($Z \in \{A,I\}$) denote the diffusion constant, decay rate, constant input, and efficacy, respectively, of the guidance cue's signal transmission, and $G(x)$ represents the guidance cue concentration at x. The activity of E was determined by the ratio of A's activity to I's, i.e., $E(x) = A(x)/I(x)$, which is reasonable if E is regulated by a push-pull enzymatic reaction between A and I [32,33]. The growth cone's migration was driven by the relative spatial polarity of E as $\Delta E/E^*$, where ΔE and E^* indicate the spatial difference of E across the growth cone (i.e., $E(L/2) - E(-L/2)$) and the baseline activity of E (i.e., $E(0)$), respectively. This property was stated as the Weber-Fechner law, in which the detectable spatial polarity of E varies because of the scale of the concentration of E [34]. Indeed, the Weber-Fechner law has been found in several types of chemotactic cells [35–40]. By analytically solving the model (see Methods), I demonstrated that it produced opposite polarities for ΔE depending on the parameters (**Fig 2C and 2D** and **Table 1**); when $\Delta E > 0$, the growth cone was attracted and migrated along the gradient, but when $\Delta E < 0$, the growth cone was repelled and turned against the gradient.

Establishment of preferred concentration by switching attraction and repulsion

I examined how chemotactic responses vary with absolute concentrations in the gradient. My previous study [27] showed that the steady-state response of $\Delta E/E^*$ was presented by

$$\frac{\Delta E}{E^*} = \frac{\Delta A}{A^*} - \frac{\Delta I}{I^*},$$

(2)

where A^* and I^* denote the baseline activities of A and I, respectively (i.e., $A^* = A(0)$ and $I^* = I(0)$), and ΔA and ΔI denote the spatial differences of A and I, respectively, across the growth cone (i.e., $\Delta A = A(L/2) - A(-L/2)$ and $\Delta I = I(L/2) - I(-L/2)$) (see **Fig 2D**). Z^* and ΔZ ($Z \in \{A, I\}$) were analytically derived (see Methods). By substituting these into Eq (2), I found that four chemotactic response patterns were generated depending on parameters (**Fig 3A and Table 1**): unidirectional repulsion, unidirectional attraction, bidirectional repulsion-to-attraction, and bidirectional attraction-to-repulsion (BAR). In the former two patterns, the growth cone always exhibited attraction or repulsion, meaning that it preferred higher or lower concentrations, respectively (**Fig 3C and 3D**). In bidirectional repulsion-to-attraction, the growth cone preferred either higher or lower concentrations depending on the initial concentration (**Fig 3B**). Finally, in BAR, the growth cone avoided both higher and lower concentrations but

Table 1. Parameters. Parameter values used in Figs 2 and 3 were listed.

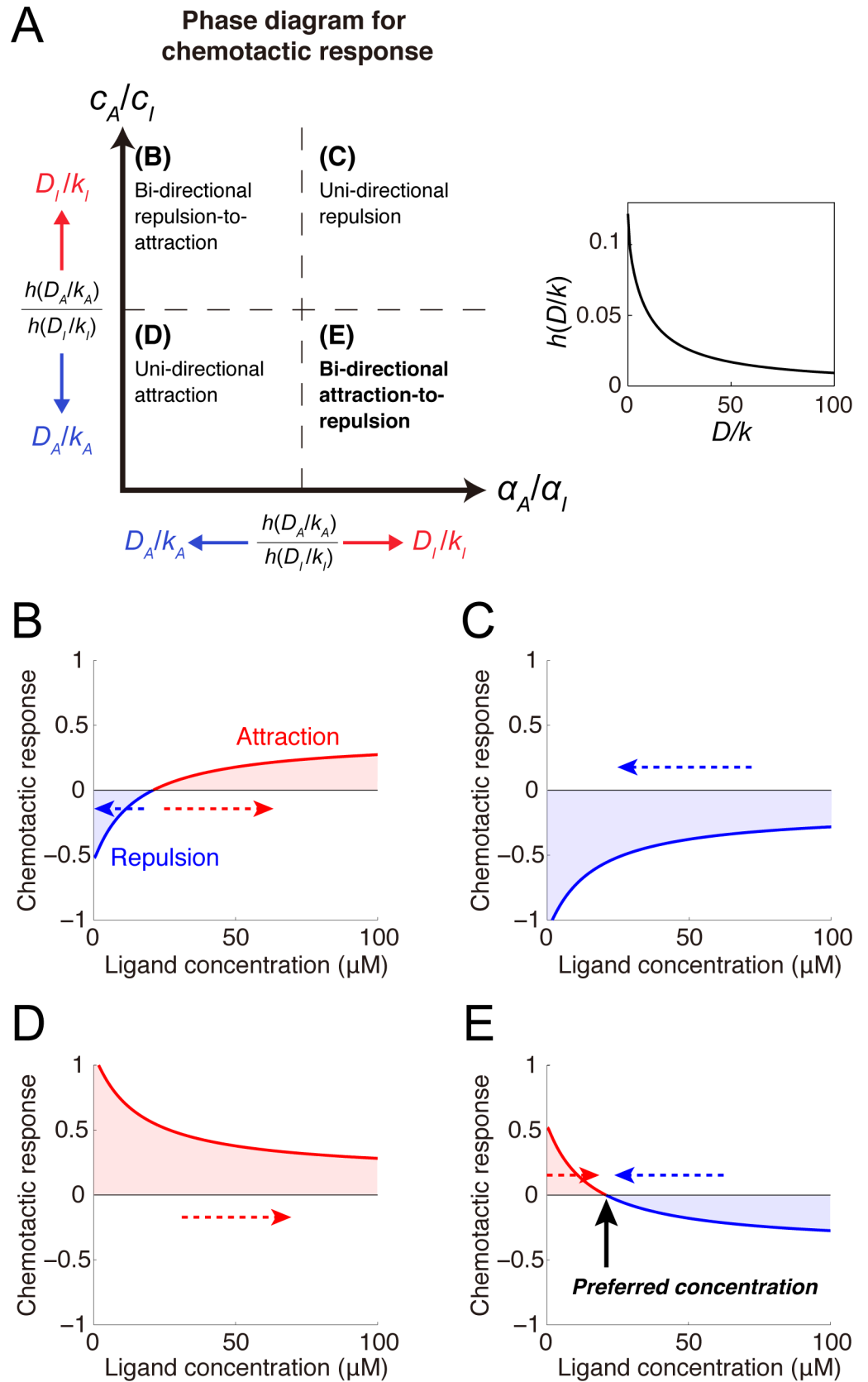| Parameter	Unit	Fig 2C	Fig 2D	Fig 3B	Fig 3C	Fig 3D	Fig 3E
L	μm	10	10	–	–	–	–
G^*	μM	10	10	–	–	–	–
g	μM/μm	0.75	0.75	–	–	–	–
D_A	μm²/s	1	100	1	20	1	20
k_A	s⁻¹	5	2	20	1	20	1
c_A	μM/s	0	0	150	0.05	150	0.05
α_A	s⁻¹	0.5	0.35	10	2.5	5	5
D_I	μm²/s	100	1	20	1	20	1
k_I	s⁻¹	2	5	1	20	1	20
c_I	μM/s	0	0	0.05	150	0.05	150
α_I	s⁻¹	0.35	0.5	5	10	5	10

Fig 3. Mechanism of ligand concentration preferences by switching attraction and repulsion. (A) Phase diagram depicting parameter regions of the four chemotactic response patterns. The dashed lines indicate critical lines corresponding to a ratio of $h(D_A/k_A)$ to $h(D_I/k_I)$. Because $h(D/k)$ is a monotonically decreasing function of D/k (inset), the critical lines move with changes in D_A/k_A and D_I/k_I. **(B-E)** Various chemotactic responses (i.e., $\Delta E/E^*$) to guidance cue concentrations were derived: **(B)** bidirectional repulsion-to-attraction, **(C)** unidirectional repulsion, **(D)** unidirectional attraction and **(E)** bidirectional attraction-to-repulsion (BAR). Dashed arrows indicate the direction of concentration changes resulting from attractive or repulsive migration. In the BAR response, the x-intercept indicated by the black arrow corresponds to the preferred guidance cue concentration. The model parameters are listed in **Table 1**.

preferred a specific concentration by switching attraction and repulsion at that concentration (**Fig 3E**). I hypothesized that this BAR pattern could play a fundamental role in topographic map formation.

Model of topographic mapping

Assuming that the growth cone exhibited the BAR pattern, I studied how receptor expression levels affected the preferred concentration. To this end, the receptor was incorporated into the model as follow:

$$
\begin{aligned}
\frac{\partial A}{\partial t} &= D_A \frac{\partial^2 A}{\partial x^2} - k_A A + c_A + \alpha_A f(R, G(x)) \\
\frac{\partial I}{\partial t} &= D_I \frac{\partial^2 I}{\partial x^2} - k_I I + c_I + \alpha_I f(R, G(x))
\end{aligned}, \tag{3}
$$

where R represents the expressed receptor's density, and $f(R,G)$ represents the density of the receptor's active form depending on the guidance cue concentration. By analyzing this model based on Eq (2) (see Methods), I found that whether the preferred concentration, G_{pref}, decreases or increases with R was determined by the sign of derivatives of $f(R,G)$ with respect to R and G:

$$
\frac{dG_{pref}}{dR} = -\frac{\partial f/\partial R}{\partial f/\partial G}. \tag{4}
$$

Therefore, $f(R,G)$, which represents how the guidance cue signal is transmitted to A and I through the receptor, is a crucial factor in the receptor expression level-dependent preferred ligand concentration. I next studied specific examples of $f(R,G)$.

Type 1 mapping encoded by EphA/ephrinA

I considered a scenario in which the receptors were activated by guidance cue binding (**Fig 4A**), which is described by $f(R,G) = RG/(K + G)$, where K is the dissociation constant of binding reaction between the receptor and guidance cue (i.e., a ratio of unbinding rate to binding rate). I then calculated the preferred concentration based on Eq (2) and found that it decreased with the receptor expression level (**Fig 4B**) as

$$
G_{pref} \propto \frac{1}{R - \gamma}, \tag{5}
$$

where γ is a positive constant determined by the model parameters. This is consistent with type 1 topographic mapping in which higher EphA levels result in the growth cone preferring smaller ephrinA concentrations (**Fig 1A and 1B**). If the receptor expression level is greater than γ, this relationship produces a linearly ordered topographic map with exponential distributions of retinal EphA and tectal ephrinA (**Fig 4C**).

Type 2 mapping encoded by EphB/ephrinB

For the mechanism of type 2 EphB/ephrinB-encoded topographic mapping, I tested two biologically plausible hypothetical $f(R,G)$ expressions. First, guidance cue-unbound receptors might trigger intracellular signaling, which can be expressed by $f(G) = RK/(K + G)$ (**Fig 4D(i)**)
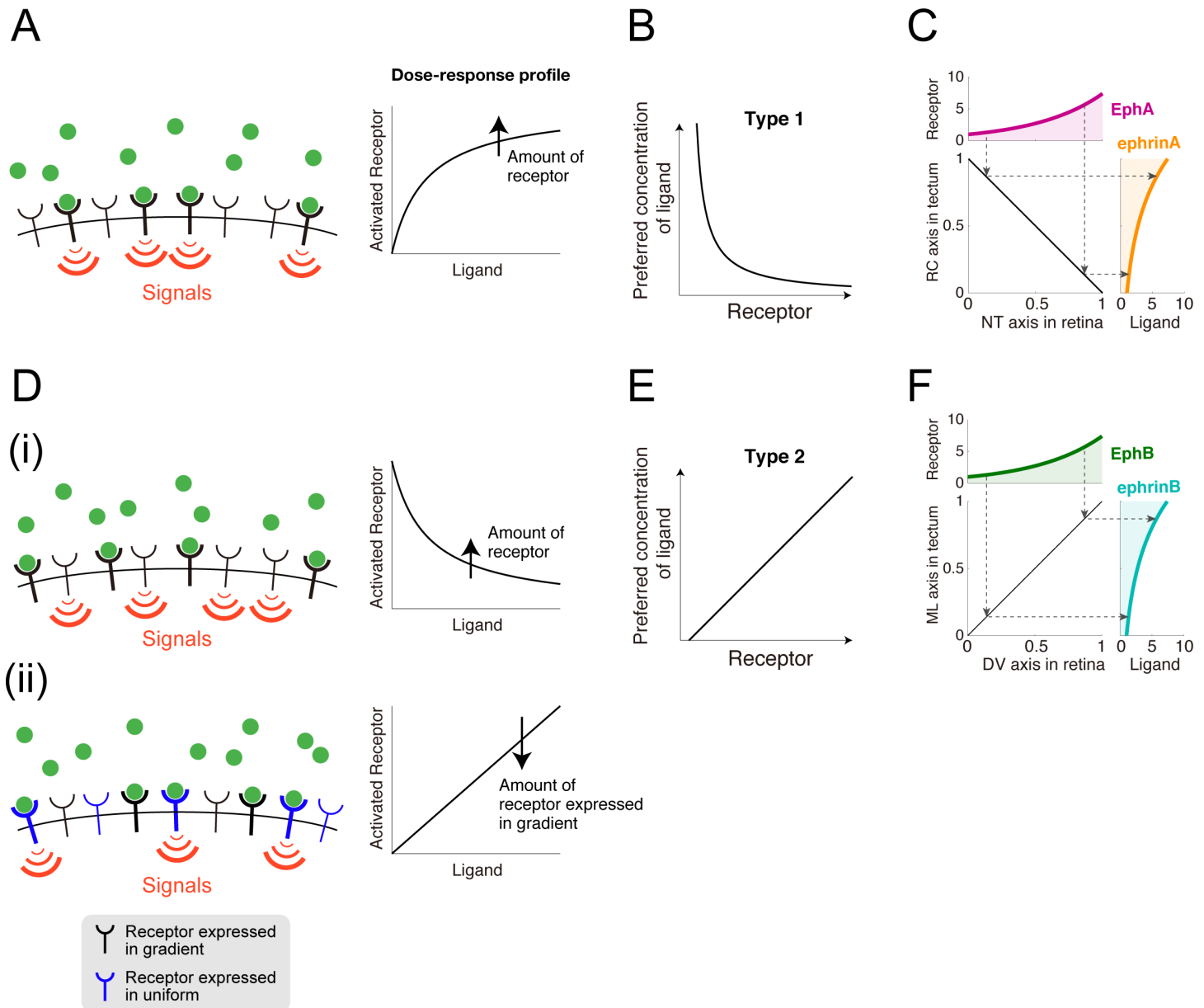

Fig 4. Topographic mapping implemented by growth cone chemotaxis. (A) The receptors were activated by guidance cue binding. Dose-response of receptor activation was plotted in right panel. **(B)** The chemotactic growth cone in (A) prefers a specific ligand concentration that is inversely proportional to the receptor expression level. **(C)** Linear topographic mapping was produced by an EphA gradient along the retinal nasal-temporal (NT) axis and an ephrinA gradient along the tectal rostral-caudal (RC) axis. Dashed arrows indicate corresponding receptor expression levels and preferred ligand concentrations. The applied gradients were $R_{NT}(x_{NT}) = R_{NT_0} exp(q_A(x_{NT}/\sigma_{NT}))$ and $G_{RC}(x_{RC}) = G_{RC_0} exp(-q_A(1 - x_{RC}/\sigma_{RC}))$. **(D)** Two possible molecular mechanisms by which the guidance cue is transduced to an intracellular signal through the receptor. **(D(i))** Guidance cue-unbound receptors were active. **(D(ii))** Two kinds of receptors competitively bind the guidance cue so that these receptors effectively suppress each other. **(E)** The chemotactic growth cone in (D) prefers a specific ligand concentration that linearly increases with the receptor expression level. **(F)** Linear topographic mapping was produced by an EphB gradient along the retinal dorsal-ventral (DV) axis and an ephrinB gradient along the tectal medial-lateral (ML) axis. The applied gradients were $R_{DV}(x_{DV}) = R_{DV_0} exp(q_B(x_{DV}/\sigma_{DV}))$ and $G_{ML}(x_{ML}) = G_{ML_0} exp(q_B(x_{ML}/\sigma_{ML}))$.

(see Discussion for its biological relevance). For this hypothesis, I found that the preferred concentration increases with the receptor expression level (Fig 4E) as

$$G_{pref} \propto R - \gamma. \tag{6}$$

This is consistent with the fact that higher EphB levels result in the growth cone preferring higher ephrinB concentrations (Fig 1C and 1D) (see Methods). This linear relationship (Eq (6)) produced a linearly ordered topographic map with exponential distributions of retinal EphB and tectal ephrinB (Fig 4F).

In the second hypothesis, I assumed that two kinds of receptor competitively bind the limited ligands (Fig 4D(ii)) (see Discussion for its biological relevance). One kind is uniformly expressed across the retina and the guidance cue-bound form triggers intracellular signaling. The other is expressed in gradients across the retina and indirectly inhibits the uniformly expressed receptor by competitively binding the ligand. This case is described by $f(R,G) = R_c G/(K + R_c + R)$ (Methods), where R and R_c indicate densities of the receptors expressed in gradients and uniformly, respectively, and K indicates the dissociation constant of the receptor and ligand. For this hypothesis, I also found that the preferred concentration increases with the receptor expression level as

$$G_{pref} \propto R + \rho, \tag{7}$$

where ρ is a positive constant determined by the model parameters. Thus, this hypothesis also explained the type 2 EphB level-dependent preferred ephrinB concentration.

Discussion

I presented a mathematical model of chemotactic response of the growth cone to reveal how topographic map is formed by the growth cone chemotaxis. In my model, for the sake of simplicity, I assumed that the migration direction of the growing axon was determined by polarity of the growth cone signaling. The real mechanism must be more complicated than what assumed in my model. However, the minimalist model I developed was very informative and provided a novel chemotaxis-based logic of chemoaffinity theory for topographic mapping. I demonstrated that the model could generate both attractive and repulsive responses depending on absolute concentrations along the gradient. Such bidirectionality endows the growth cone with the preference for a specific guidance cue concentration by switching between attraction and repulsion around that concentration. I also determined the conditions of EphA/ephrinA- and EphB/ephrinB-encoded topographic mapping, in which the preferred concentration decreases and increases, respectively, with the receptor expression level. This study therefore redefined Sperry's chemoaffinity theory in terms of chemotaxis.

Ephrins as attractants and repellents

If ephrinA is a repellent, as classically thought [41], then all RGC growth cones must project to the tectum's rostral end, which has the lowest ephrinA concentration. However, this is not the case; even without tectal space competition between projecting axons, the RGC axons project to the correct terminal zone in the tectum [42]. This contradiction can be resolved simply by regarding ephrinA as both an attractant and a repellent. In fact, ephrinA has been reported to be an attractant or a repellent in a concentration-dependent manner [11]. EphrinB has been regarded as both an attractant and a repellent [12,13]. However, their underlying mechanism was largely unknown. In this study, I demonstrated how ephrinA and ephrinB could indeed work as both attractants and repellents for the chemotactic growth cone.

Signal transmission through EphA and EphB

I demonstrated that whether the preferred ligand concentration decreases or increases with the receptor expression level is determined by whether the guidance cue and the receptor positively or negatively affect intracellular signaling (Eq (4)). As the mechanism of EphA/ephrinA-encoded type 1 topographic mapping, I reasonably assumed that ephrinA-bound EphAs trigger intracellular signaling (**Fig 4A**), but for type 2 topographic mapping, I tested two hypothetical EphB/ephrinB regulation schemes. The first hypothesis was that ephrinB-unbound EphBs, rather than bound ones, trigger intracellular signaling (**Fig 4D(i)**). This seems inconsistent with a property of tyrosine kinase-type receptors, which are activated by ligand binding through phosphorylation [43,44], but it has recently been reported that Ephs can be ligand-independently activated by hemophilic Eph-Eph interactions [45], suggesting that ephrinB-bound and -unbound EphBs could generate different signals. The first hypothesis was thus biologically feasible, but further experimental investigation is needed. The second hypothesis was that two kinds of receptor, which are expressed uniformly or in gradients across the retina, competitively bind the ligand (**Fig 4D(ii)**). This fits the expression profiles of EphB subtypes in the chicken retina well; EphB2 and EphB3 are expressed in gradients across the retina, whereas EphB1 is uniformed expressed [7]. My hypothesis thus offers experimentally testable predictions concerning EphB/ephrinB regulation.

Functional difference between two types of topographic mappings

It is worth mentioning functional difference between type 1 and type 2 of topographic mappings. I deduced that local accuracy of axonal projection is determined by multiplication of three factors: 1. spatial derivatives of receptor expression profile in retina (upper panels in **Fig 4C and 4F**), 2. steepness of mapping function from receptor expression to preferred ligand concentration (**Fig 4B and 4E**) and 3. spatial derivatives of ligand in tectum (right panels in **Fig 4C and 4F**). In type 1 topographic mapping, while multiplication of the first and third factors, i.e., $(dR_{NT}/dx_{NT})(dG_{RC}/dx_{RC})$, is constant (**Fig 4C**), the second factor, i.e., the steepness of mapping function, increases as EphA expression decreases (**Fig 4B**). On the other hand, in type 2 topographic mapping, while the second factor, i.e., the steepness of mapping function, is constant (**Fig 4E**), multiplication of the first and third factors, i.e., $(dR_{DV}/dx_{DV})(dG_{ML}/dx_{ML})$, increases with EphB expression. Thus, it can be predicted that axonal projection from nasal ventral retinal region associated with lower EphA and higher EphB expression could be more precise than that other retinal region.

Species-dependent pattern of axonal projections

RGCs' axonal projection patterns in the optic tectum or SC are species-dependent. In higher vertebrates (i.e., mammals and birds), the axons overshoot their terminal zones and subsequently form branches [7], while in lower vertebrates (i.e., fish and amphibians), the growth cones directly reach and stop in their terminal zones [7] despite being initially misrouted [46]. The latter case suggests that the chemotactic system implements chemoaffinity, which I investigated as the mechanism of topographic mapping. The growth cone's chemotaxis might therefore play a fundamental role in topographic mapping, while axonal overshoot and branching might facilitate exploration of the terminal zone. My model could understand the axonal overshoot by incorporating transient dynamics of activator and inhibitor, instead of steady state assumption. On the other hand, how the axon generates branches is out of scope of my model.

Comparison with previous chemotaxis models

Chemotactic gradient sensing has been computationally studied mainly for non-neural chemotactic cells [40,47–51] like *Dictyostelium discoideum* and immune cells, though attraction to guidance cues has been only paid attention. On the other hand, there are a couple of computational models for the growth cone chemotaxis alternating attraction and repulsion [27, 52]. These models, whether applied to neural or non-neural cells, primarily addressed intracellular signaling consisting of activators and inhibitors. In the non-neural cells, the activator and inhibitor were thought to be PI3K and PTEN [28], respectively, or RasGEF and RasGAP [29], respectively. In the growth cone, CaMKII and PP1 were thought to work as the activator and inhibitor, respectively [27,30,31,52], which regulate cellular motility via Rho GTPases [53]. In short, chemotactic responses could be understood from the activator-inhibitor framework [54], so I hypothesized that RGC chemotaxis is also regulated by an activator-inhibitor system, although the intracellular signaling pathway of Eph/ephrin has not been fully identified.

Comparison with previous models of topographic mapping

There have been many computational studies on topographic mapping [14]. These studies did not focus on the intracellular mechanism of growth cone chemotaxis, but instead developed models with heuristically designed chemoaffinity (e.g., optimization of energy function) by which the growth cone reaches its correct terminal zone. Given such chemoaffinity, these models potentially gave insights into more system-level phenomena, such as abnormal maps resulting from surgical experiments in the retinotectal system [15–17] and from the misexpression of Eph or ephrin [15,18–25]. These models included several factors not included in my model, such as axon competition for tectal space [55] and counter-gradients of Ephs and ephrins in the retina and tectum [56]. Several models have also addressed a question of how synaptic connection is refined by activity-dependent synaptic plasticity mechanism after activity-independent axon guidance [20,57–59]. Therefore, I must stress that my model does not compete with previous models, but rather can explain the underlying mechanism by which growth cones can chemotactically implement the previous models' heuristically designed chemoaffinity.

Methods

Theory for chemotactic response

Suppose a shallow extracellular gradient because growth cones are known to detect few percent difference of concentrations across the growth cone [60–64]. I then assumed that the intracellular gradients of A and I, $A(x)$ and $I(x)$, were shallow and slightly perturbed from their activities at $x = 0$. The activity of E at x could be linearized as

$$E(x) \simeq E^* + \frac{1}{I^*}[A(x) - A^*] - \frac{A^*}{I^{*2}}[I(x) - I^*], \tag{8}$$

where $A^* = A(0)$, $I^* = I(0)$, and $E^* = E(0) = A^*/I^*$. The relative spatial difference of E across the growth cone was calculated by

$$\frac{\Delta E}{E^*} \equiv \frac{E(L/2) - E(-L/2)}{E(0)} = \frac{\Delta A}{A^*} - \frac{\Delta I}{I^*}, \tag{9}$$

where ΔA and ΔI indicate the spatial differences of A and I, respectively, across the growth cone.

Distribution of A and I

For both A and I, I calculated the intracellular distribution exposure to an extracellular gradient, $G(x)$. Green's function of $\partial Z/\partial t = D_z(\partial^2 Z/\partial x^2) - k_z Z$ was analytically derived using the method of separation of variables:

$$H(x, \xi, t) = \frac{1}{L}\exp(-k_z t)$$
$$+ \frac{2}{L}\sum_{n=1}^{\infty}\cos\left[\frac{n\pi}{L}\left(\xi + \frac{L}{2}\right)\right]\cos\left[\frac{n\pi}{L}\left(x + \frac{L}{2}\right)\right]\exp\left[-\left\{k_z + \left(\frac{n\pi}{L}\right)^2 D_z\right\}t\right]. \quad (10)$$

A steady-state solution of Eq (3) was thus obtained by

$$Z^{\infty}(x) = \int_0^{\infty} d\tau \int_{-L/2}^{+L/2} d\xi H(x, \xi, \tau)\{c_z + \alpha_z f(R, G(\xi))\}, \quad (11)$$

where Z represents either A or I. Note that $f(R,G(x)) = G(x)$ in Eq (1). Because the growth cone is so small that $G(x)$ could be modelled as a shallow linear gradient, $f(R,G(x))$ can be linearized by $f(R,G^*) + gx$, where $G^* = G(0)$ and $g = (\partial f/\partial G|_{G = G^*})(dG/dx|_{x = 0})$. This led to

$$Z^{\infty}(x) = Z^* + \frac{2g}{L}\sum_{n=1}^{\infty}\frac{(L/n\pi)^2[(-1)^n - 1]}{k_z + (n\pi/L)^2 D_z}\cos\left\{\frac{n\pi}{L}\left(x + \frac{L}{2}\right)\right\}, \quad (12)$$

where Z^* indicates baseline activity, i.e., $Z^* = Z^{\infty}(0)$:

$$Z^* = \frac{\alpha_z f(R, G^*) + c_z}{k_z}. \quad (13)$$

By numerical simulation of the reaction-diffusion dynamics, I confirmed that Eq (12) was exact. The spatial difference of Z then becomes

$$\Delta Z = Z^{\infty}(L/2) - Z^{\infty}(-L/2) = \frac{8gL^3}{\pi^4}\frac{h(D_z/k_z)}{k_z}, \quad (14)$$

where

$$h(s) = \sum_{n=1}^{\infty}\frac{1/(2n + 1)^2}{(2n + 1)^2 s + (L/\pi)^2}, \quad (15)$$

which is a monotonically decreasing function converging to 0 (inset of **Fig 3A**).

Conditions for four chemotactic response patterns

I calculated the growth cone's concentration-dependent chemotactic responses. By substituting Z^* as described by Eq (13) for A^* and I^* in Eq (2) and substituting ΔZ as described by Eq (14) for ΔA and ΔI in Eq (2), I obtained

$$\frac{\Delta E}{E^*} = \frac{8gL^3}{\pi^4}\left[\frac{h(D_A/k_A)}{\alpha_A f(R, G^*) + c_A} - \frac{h(D_I/k_I)}{\alpha_I f(R, G^*) + c_I}\right]. \quad (16)$$

Eq (16) exhibits four response patterns to G^*: all positive, all negative, negative-to-positive, and positive-to-negative, which correspond to unidirectional attraction, unidirectional repulsion, bidirectional repulsion-to-attraction, and BAR, respectively (**Fig 3B–3E**). The response patterns' parameter regions were derived under the condition of $\partial f/\partial G > 0$ (**Fig 3A**). For example, the BAR response pattern is characterized by attraction at lower concentrations (i.e.,

$\Delta E/E^*|_{G^* = 0} > 0$) and repulsion at $G^* = \infty$ (i.e., $\Delta E/E^*|_{G^* = 0} < 0$), which leads to

$$\frac{c_A}{c_I} < \eta < \frac{\alpha_A}{\alpha_I}, \tag{17}$$

where $\eta = h(D_A/k_A)/h(D_I/k_I)$.

Preferred concentration in the BAR response pattern

Growth cones with the BAR response pattern prefer a specific concentration of G^* at which $\Delta E/E^* = 0$. In the Eq (3) model, setting $\Delta E/E^* = 0$ in Eq (16) leads to

$$f(R, G_{pref}) = \gamma, \tag{18}$$

where $\gamma = (\eta c_I - c_A)/(\alpha_A - \eta \alpha_I)$. The preferred concentration with a specific $f(R,G)$ can be calculated with Eq (18). In the Eq (1) model, $f(R,G) = G$, thus $G_{pref} = \gamma$. If $f(R,G) = RG/(K + G)$, $G_{pref} = \gamma K/(R - \gamma)$ (Eq (5); **Fig 4A**). If $f(R,G) = RK/(K + G)$, $G_{pref} = (K/\gamma)(R - \gamma)$ (Eq (6); **Fig 4D (i)**). If $f(R,G) = R_c G/(K + R_c + R)$, $G_{pref} = (\gamma/R_c)/(R + K + R_c)$ (Eq (7); **Fig 4D(ii)**). Total differentiation of Eq (18) leads to $(\partial f/\partial R)dR + (\partial f/\partial G_{pref})dG_{pref} = 0$, which in turn leads to

$$\frac{dG_{pref}}{dR} = -\frac{\partial f / \partial R}{\partial f / \partial G}. \tag{19}$$

Competitive binding of limited ligands by two receptors

I assumed a scenario in which two kinds of RGC-expressed receptors competitively bind limited ligands with identical kinetics. Note that the two assumed kinds are expressed either uniformly or in gradients across the retina. Such dynamics are described by

$$\begin{aligned} \frac{dR_c^*}{dt} &= k_f(R_c - R_c^*)G_f - k_b R_c^* \\ \frac{dR_g^*}{dt} &= k_f(R_g - R_g^*)G_f - k_b R_g^* \end{aligned}, \tag{20}$$

where R_j, R_j^*, and $G_f (j \in \{c,g\})$ indicate densities of the total receptors, guidance cue-bound receptors, and free guidance cues, respectively, and k_f and k_b indicate forward and backward reaction rates, respectively. The total guidance cue concentration is conserved as $G = G_f + R_c^* + R_g^*$. At steady state, $R_j^* = R_j G_f/(K + G_f)$, where $K = k_b/k_f$. If $K \gg G_f$, R_j^* can be approximated as $(R_j/K)G_f$, and the steady state of R_c^* depending on G is then described by

$$R_c^* = \frac{R_c G}{K + R_c + R_g}. \tag{21}$$

Acknowledgments

Author Contributions

Conceptualization: Honda Naoki.

Data curation: Honda Naoki.

Formal analysis: Honda Naoki.

Funding acquisition: Honda Naoki.

Investigation: Honda Naoki.

Methodology: Honda Naoki.

Project administration: Honda Naoki.

Resources: Honda Naoki.

Software: Honda Naoki.

Supervision: Honda Naoki.

Validation: Honda Naoki.

Visualization: Honda Naoki.

Writing – original draft: Honda Naoki.

Writing – review & editing: Honda Naoki.

References

1. Arimura N, Kaibuchi K. Neuronal polarity: from extracellular signals to intracellular mechanisms. Nat Rev Neurosci. 2007; 8: 194–205. https://doi.org/10.1038/nrn2056 PMID: 17311006

2. Naoki H, Nakamuta S, Kaibuchi K, Ishii S. Flexible search for single-axon morphology during neuronal spontaneous polarization. PLoS One. 2011; 6. https://doi.org/10.1371/journal.pone.0019034 PMID: 21559492

3. Takano T, Wu M, Nakamuta S, Naoki H, Ishizawa N, Namba T, et al. Discovery of long-range inhibitory signaling to ensure single axon formation. https://doi.org/10.1038/s41467-017-00044-2 PMID: 28652571

4. Dickson BJ. Molecular mechanisms of axon guidance. Science (80-). 2002; 298: 1959–1964. https://doi.org/10.1126/science.1072165 PMID: 12471249

5. Kennedy TE, Wang H, Marshall W, Tessier-Lavigne M. Axon Guidance by Diffusible Chemoattractants: A Gradient of Netrin Protein in the Developing Spinal Cord. J Neurosci. 2006; 26: 8866–8874. https://doi.org/10.1523/JNEUROSCI.5191-05.2006 PMID: 16928876

6. Colamarino SA, Tessier-Lavigne M. The axonal chemoattractant netrin-1 is also a chemorepellent for trochlear motor axons. Cell. 1995; 81: 621–9. Available: http://www.ncbi.nlm.nih.gov/pubmed/7758116 PMID: 7758116

7. McLaughlin T, O'Leary DDM. Molecular gradients and development of retinotopic maps. Annu Rev Neurosci. 2005; 28: 327–55. https://doi.org/10.1146/annurev.neuro.28.061604.135714 PMID: 16022599

8. Sperry RWW. Chemoaffinity in the orderly growth of nerve fiber patterns and connections. Proc Natl Acad Sci U S A. National Academy of Sciences; 1963; 50: 703. https://doi.org/10.1073/pnas.50.4.703

9. Cheng HJ, Nakamoto M, Bergemann AD, Flanagan JG. Complementary gradients in expression and binding of ELF-1 and Mek4 in development of the topographic retinotectal projection map. Cell. 1995; 82: 371–381. https://doi.org/10.1016/0092-8674(95)90426-3 PMID: 7634327

10. Drescher U, Kremoser C, Handwerker C, Löschinger J, Noda M, Bonhoeffer F. In vitro guidance of retinal ganglion cell axons by RAGS, a 25 kDa tectal protein related to ligands for Eph receptor tyrosine kinases. Cell. 1995; 82: 359–370. https://doi.org/10.1016/0092-8674(95)90425-5 PMID: 7634326

11. Hansen MJ, Dallal GE, Flanagan JG. Retinal axon response to ephrin-As shows a graded, concentration-dependent transition from growth promotion to inhibition. Neuron. 2004; 42: 717–730. https://doi.org/10.1016/j.neuron.2004.05.009 PMID: 15182713

12. McLaughlin T, Hindges R, Yates P a, O'Leary DDM. Bifunctional action of ephrin-B1 as a repellent and attractant to control bidirectional branch extension in dorsal-ventral retinotopic mapping. Development. 2003; 130: 2407–2418. https://doi.org/10.1242/dev.00467 PMID: 12702655

13. Matsuoka H, Obama H, Kelly ML, Matsui T, Nakamoto M. Biphasic functions of the kinase-defective Ephb6 receptor in cell adhesion and migration. J Biol Chem. 2005; 280: 29355–29363. https://doi.org/10.1074/jbc.M500010200 PMID: 15955811

14. Goodhill G, Xu J. The development of retinotectal maps: a review of models based on molecular gradients. Netw Comput Neural Syst. 2005; Available: http://www.tandfonline.com/doi/abs/10.1080/09548980500254654

15. Gebhardt C, Bastmeyer M, Weth F. Balancing of ephrin/Eph forward and reverse signaling as the driving force of adaptive topographic mapping. Development. 2012; 139: 335–45. https://doi.org/10.1242/dev.070474 PMID: 22159582

16. Fraser SE, Perkel DH. Competitive and positional cues in the patterning of nerve connections. J Neurobiol. 1990; 21: 51–72. https://doi.org/10.1002/neu.480210105 PMID: 2181067

17. Whitelaw VA, Cowan JD. Specificity and plasticity of retinotectal connections: a computational model. J Neurosci. 1981; 1: 1369–1387. PMID: 7320751

18. Honda H. Competition between retinal ganglion axons for targets under the servomechanism model explains abnormal retinocollicular projection of Eph receptor-overexpressing or ephrin-lacking mice. J Neurosci. 2003; 23: 10368–77. 23/32/10368 [pii] PMID: 14614096

19. Koulakov A a Tsigankov DN. A stochastic model for retinocollicular map development. BMC Neurosci. 2004; 5: 30. https://doi.org/10.1186/1471-2202-5-30 PMID: 15339341

20. Tsigankov DN, Koulakov AA. A unifying model for activity-dependent and activity-independent mechanisms predicts complete structure of topographic maps in ephrin-A deficient mice. J Comput Neurosci. 2006; 21: 101–114. https://doi.org/10.1007/s10827-006-9575-7 PMID: 16823525

21. Tsigankov D, Koulakov A a. Sperry versus Hebb: topographic mapping in Isl2/EphA3 mutant mice. BMC Neurosci. BioMed Central Ltd; 2010; 11: 155. https://doi.org/10.1186/1471-2202-11-155 PMID: 21190559

22. Owens MT, Feldheim DA, Stryker MP, Triplett JW. Stochastic Interaction between Neural Activity and Molecular Cues in the Formation of Topographic Maps. Neuron. Elsevier Inc.; 2015; 87: 1261–1273. https://doi.org/10.1016/j.neuron.2015.08.030 PMID: 26402608

23. Yates PA, Holub AD, McLaughlin T, Sejnowski TJ, O'Leary DDM. Computational Modeling of Retinotopic Map Development to Define Contributions of EphA-EphrinA Gradients, Axon-Axon Interactions, and Patterned Activity. J Neurobiol. 2004; 59: 95–113. https://doi.org/10.1002/neu.10341 PMID: 15007830

24. Godfrey KB, Swindale N V. Modeling development in retinal afferents: retinotopy, segregation, and ephrinA/EphA mutants. PLoS One. 2014; 9: e104670. https://doi.org/10.1371/journal.pone.0104670 PMID: 25122119

25. Grimbert F, Cang J. New model of retinocollicular mapping predicts the mechanisms of axonal competition and explains the role of reverse molecular signaling during development. J Neurosci. 2012; 32: 9755–9768. https://doi.org/10.1523/JNEUROSCI.6180-11.2012 PMID: 22787061

26. Hopker VH, Shewan D, Tessier-Lavigne M, Poo M, Holt C. Growth-cone attraction to netrin-1 is converted to repulsion by laminin-1. Nature. 1999; 401: 69–73. https://doi.org/10.1038/43441 PMID: 10485706

27. Naoki H, Nishiyama M, Togashi K, Igarashi Y, Hong K, Ishii S. Multi-phasic bi-directional chemotactic responses of the growth cone. Sci Rep. Nature Publishing Group; 2016; 6: 36256. https://doi.org/10.1038/srep36256 PMID: 27808115

28. Janetopoulos C, Ma L, Devreotes PN, Iglesias P a. Chemoattractant-induced phosphatidylinositol 3,4,5-trisphosphate accumulation is spatially amplified and adapts, independent of the actin cytoskeleton. Proc Natl Acad Sci U S A. 2004; 101: 8951–8956. https://doi.org/10.1073/pnas.0402152101 PMID: 15184679

29. Takeda K, Shao D, Adler M, Charest PG, Loomis WF, Levine H, et al. Incoherent Feedforward Control Governs Adaptation of Activated Ras in a Eukaryotic Chemotaxis Pathway. Sci Signal. 2012; 5: ra2–ra2. https://doi.org/10.1126/scisignal.2002413 PMID: 22215733

30. Wen Z, Guirland C, Ming GL, Zheng JQ. A CaMKII/calcineurin switch controls the direction of Ca^{2+}-dependent growth cone guidance. Neuron. 2004; 43: 835–846. https://doi.org/10.1016/j.neuron.2004.08.037 PMID: 15363394

31. Gomez TM, Zheng JQ. The molecular basis for calcium-dependent axon pathfinding. Nat Rev Neurosci. 2006; 7: 115–125. https://doi.org/10.1038/nrn1844 PMID: 16429121

32. Ferrell JE. Tripping the switch fantastic: How a protein kinase cascade can convert graded inputs into switch-like outputs. Trends in Biochemical Sciences. 1996. pp. 460–466. https://doi.org/10.1016/S0968-0004(96)20026-X PMID: 9009826

33. Goldbeter A, Koshland DE. An amplified sensitivity arising from covalent modification in biological systems. Proc Natl Acad Sci U S A. 1981; 78: 6840–6844. https://doi.org/10.1073/pnas.78.11.6840 PMID: 6947258

34. Keller EF, Segel LA. Traveling bands of chemotactic bacteria: A theoretical analysis. J Theor Biol. 1971; 30: 235–248. https://doi.org/10.1016/0022-5193(71)90051-8 PMID: 4926702

35. Van Haastert PJM. Sensory adaptation of Dictyostelium discoideum cells to chemotactic signals. J Cell Biol. 1983; 96: 1559–1565. https://doi.org/10.1083/jcb.96.6.1559 PMID: 6304109

36. Adler M, Mayo A, Alon U. Logarithmic and Power Law Input-Output Relations in Sensory Systems with Fold-Change Detection. PLoS Comput Biol. 2014; 10. https://doi.org/10.1371/journal.pcbi.1003781 PMID: 25121598

37. Keller HU, Wissler JH, Hess MW, Cottier H. Distinct chemokinetic and chemotactic responses in neutrophil granulocytes. Eur J Immunol. 1978; 8: 1–7. https://doi.org/10.1002/eji.1830080102 PMID: 639837

38. Levit MN, Stock JB. Receptor Methylation Controls the Magnitude of Stimulus-Response Coupling in Bacterial Chemotaxis. J Biol Chem. 2002; 277: 36760–36765. https://doi.org/10.1074/jbc.M204325200 PMID: 12119291

39. Lazova MD, Ahmed T, Bellomo D, Stocker R, Shimizu TS. Response rescaling in bacterial chemotaxis. Proc Natl Acad Sci U S A. National Academy of Sciences; 2011; 108: 13870–5. https://doi.org/10.1073/pnas.1108608108 PMID: 21808031

40. Kamino K, Kondo Y. Rescaling of spatio-temporal sensing in eukaryotic chemotaxis. PLoS One. 2016; 11. https://doi.org/10.1371/journal.pone.0164674 PMID: 27792738

41. Nakamoto M, Cheng HJ, Friedman GC, McLaughlin T, Hansen MJ, Yoon CH, et al. Topographically specific effects of ELF-1 on retinal axon guidance in vitro and retinal axon mapping in vivo. Cell. 1996; 86: 755–766. https://doi.org/10.1016/S0092-8674(00)80150-6 PMID: 8797822

42. Gosse NJ, Nevin LM, Baier H. Retinotopic order in the absence of axon competition. Nature. 2008; 452: 892–5. https://doi.org/10.1038/nature06816 PMID: 18368050

43. Kania A, Klein R. Mechanisms of ephrin-Eph signalling in development, physiology and disease. Nat Rev Mol Cell Biol. 2016; 17: 240–56. https://doi.org/10.1038/nrm.2015.16 PMID: 26790531

44. Wilkinson DG. Multiple roles of EPH receptors and ephrins in neural development. Nat Rev Neurosci. 2001; 2: 155–64. https://doi.org/10.1038/35058515 PMID: 11256076

45. Nikolov DB, Xu K, Himanen JP. Homotypic receptor-receptor interactions regulating Eph signaling. Cell Adhesion and Migration. 2014. pp. 360–365. https://doi.org/10.4161/19336918.2014.971684 PMID: 25530219

46. Fujisawa H, Tani N, Watanabe K, Ibata Y. Branching of regenerating retinal axons and preferential selection of appropriate branches for specific neuronal connection in the newt. Dev Biol. 1982; 90: 43–57. https://doi.org/10.1016/0012-1606(82)90210-X PMID: 7060834

47. Naoki H, Sakumura Y, Ishii S. Stochastic control of spontaneous signal generation for gradient sensing in chemotaxis. J Theor Biol. 2008; 255: 259–266. https://doi.org/10.1016/j.jtbi.2008.08.012 PMID: 18789338

48. Levchenko A, Iglesias PA. Models of eukaryotic gradient sensing: application to chemotaxis of amoebae and neutrophils. Biophys J. 2002; 82: 50–63. https://doi.org/10.1016/S0006-3495(02)75373-3 PMID: 11751295

49. Nakajima A, Ishihara S, Imoto D, Sawai S. Rectified directional sensing in long-range cell migration. Nat Commun. 2014; 5: 5367. https://doi.org/10.1038/ncomms6367 PMID: 25373620

50. Xiong Y, Huang C-H, Iglesias PA, Devreotes PN. Cells navigate with a local-excitation, global-inhibition-biased excitable network. Proc Natl Acad Sci U S A. 2010; 107: 17079–86. https://doi.org/10.1073/pnas.1011271107 PMID: 20864631

51. Nonaka S, Naoki H, Ishii S. A multiphysical model of cell migration integrating reaction-diffusion, membrane and cytoskeleton. Neural Networks. Elsevier Ltd; 2011; 24: 979–989. https://doi.org/10.1016/j.neunet.2011.06.009 PMID: 21764259

52. Forbes EM, Thompson AW, Yuan J, Goodhill GJ. Calcium and cAMP Levels Interact to Determine Attraction versus Repulsion in Axon Guidance. Neuron. 2012; 74: 490–503. https://doi.org/10.1016/j.neuron.2012.02.035 PMID: 22578501

53. Yamao M, Naoki H, Kunida K, Aoki K, Matsuda M, Ishii S. Distinct predictive performance of Rac1 and Cdc42 in cell migration. Sci Rep. Nature Publishing Group; 2015; 5: 17527. https://doi.org/10.1038/srep17527 PMID: 26634649

54. Mortimer D, Fothergill T, Pujic Z, Richards LJ, Goodhill GJ. Growth cone chemotaxis. Trends in Neurosciences. 2008. pp. 90–98. https://doi.org/10.1016/j.tins.2007.11.008 PMID: 18201774

55. Brown A, Yates PA, Burrola P, Ortuñ D, Vaidya A, Jessell TM, et al. Topographic Mapping from the Retina to the Midbrain Is Controlled by Relative but Not Absolute Levels of EphA Receptor Signaling RGC axons, most strongly for those that originate in the. Cell. 2000; 102: 77–88. https://doi.org/10.1016/S0092-8674(00)00012-X PMID: 10929715

56. Yates P a, Roskies a L, McLaughlin T, O'Leary DD. Topographic-specific axon branching controlled by ephrin-As is the critical event in retinotectal map development. J Neurosci. 2001; 21: 8548–8563. 21/21/8548 [pii] PMID: 11606643

57. Debski EA, Cline HT. Activity-dependent mapping in the retinotectal projection. Current Opinion in Neurobiology. 2002. pp. 93–99. https://doi.org/10.1016/S0959-4388(02)00295-7 PMID: 11861170

58. van Ooyen a. Competition in the development of nerve connections: a review of models. Network. 2001; 12: R1–R47. https://doi.org/10.1080/net.12.1.1.47 PMID: 11254084

59. Willshaw DJ, von der Malsburg C. How patterned neural connections can be set up by self-organization. Proc R Soc London Ser B, Biol Sci. 1976; 194: 431–45. https://doi.org/10.1098/rspb.1976.0087

60. Bagnard D, Thomasset N, Lohrum M, Püschel a W, Bolz J. Spatial distributions of guidance molecules regulate chemorepulsion and chemoattraction of growth cones. J Neurosci. 2000; 20: 1030–1035. PMID: 10648708

61. Goodhill GJ, Baier H. Axon guidance: stretching gradients to the limit. Neural Comput. 1998; 10: 521–527. https://doi.org/10.1162/089976698300017638 PMID: 9527831

62. Xu J, Rosoff WJ, Urbach JS, Goodhill GJ. Adaptation is not required to explain the long-term response of axons to molecular gradients. Development. 2005; 132: 4545–52. https://doi.org/10.1242/dev.02029 PMID: 16176951

63. Baier H, Bonhoeffer F. Axon guidance by gradients of a target-derived component. Sci (New York, NY). 1992; 255: 472–475. https://doi.org/10.1126/science.1734526

64. Mortimer D, Pujic Z, Vaughan T, Thompson AW, Feldner J, Vetter I, et al. Axon guidance by growth-rate modulation. Proc Natl Acad Sci U S A. 2010; 107: 5202–5207. https://doi.org/10.1073/pnas.0909254107 PMID: 20194766